Mechanical and chemical element structures of sea urchin spines for locomotion and defense (#110526)

First revision

Guidance from your Editor

Please submit by **25 Jun 2025** for the benefit of the authors (and your token reward) .

Structure and Criteria
Please read the 'Structure and Criteria' page for guidance.

Raw data check
Review the raw data.

Image check
Check that figures and images have not been inappropriately manipulated.

All review materials are strictly confidential. Uploading the manuscript to third-party tools such as Large Language Models is not allowed.
If this article is published your review will be made public. You can choose whether to sign your review. If uploading a PDF please remove any identifiable information (if you want to remain anonymous).

Files

Download and review all files from the materials page.

1 Tracked changes manuscript(s)
1 Rebuttal letter(s)
9 Figure file(s)
2 Table file(s)
7 Raw data file(s)

Structure and Criteria

Structure your review

The review form is divided into 5 sections. Please consider these when composing your review:

1. **BASIC REPORTING**
2. **EXPERIMENTAL DESIGN**
3. **VALIDITY OF THE FINDINGS**
4. General comments
5. Confidential notes to the editor

You can also annotate this PDF and upload it as part of your review

When ready submit online.

Editorial Criteria

Use these criteria points to structure your review. The full detailed editorial criteria is on your guidance page.

BASIC REPORTING

- Clear, unambiguous, professional English language used throughout.
- Intro & background to show context. Literature well referenced & relevant.
- Structure conforms to PeerJ standards, discipline norm, or improved for clarity.
- Figures are relevant, high quality, well labelled & described.
- Raw data supplied (see PeerJ policy).

EXPERIMENTAL DESIGN

- Original primary research within Scope of the journal.
- Research question well defined, relevant & meaningful. It is stated how the research fills an identified knowledge gap.
- Rigorous investigation performed to a high technical & ethical standard.
- Methods described with sufficient detail & information to replicate.

VALIDITY OF THE FINDINGS

- **Impact and novelty is not assessed.** Meaningful replication encouraged where rationale & benefit to literature is clearly stated.
- All underlying data have been provided; they are robust, statistically sound, & controlled.
- Conclusions are well stated, linked to original research question & limited to supporting results.

Standout reviewing tips

The best reviewers use these techniques

Tip	*Example*
Support criticisms with evidence from the text or from other sources	*Smith et al (J of Methodology, 2005, V3, pp 123) have shown that the analysis you use in Lines 241-250 is not the most appropriate for this situation. Please explain why you used this method.*
Give specific suggestions on how to improve the manuscript	*Your introduction needs more detail. I suggest that you improve the description at lines 57- 86 to provide more justification for your study (specifically, you should expand upon the knowledge gap being filled).*
Comment on language and grammar issues	*The English language should be improved to ensure that an international audience can clearly understand your text. Some examples where the language could be improved include lines 23, 77, 121, 128 – the current phrasing makes comprehension difficult. I suggest you have a colleague who is proficient in English and familiar with the subject matter review your manuscript, or contact a professional editing service.*
Organize by importance of the issues, and number your points	*1. Your most important issue* *2. The next most important item* *3. …* *4. The least important points*
Please provide constructive criticism, and avoid personal opinions	*I thank you for providing the raw data, however your supplemental files need more descriptive metadata identifiers to be useful to future readers. Although your results are compelling, the data analysis should be improved in the following ways: AA, BB, CC*
Comment on strengths (as well as weaknesses) of the manuscript	*I commend the authors for their extensive data set, compiled over many years of detailed fieldwork. In addition, the manuscript is clearly written in professional, unambiguous language. If there is a weakness, it is in the statistical analysis (as I have noted above) which should be improved upon before Acceptance.*

PeerJ Chemistry Journals
Analytical, Inorganic, Organic, Physical, Materials Science

Manuscript to be reviewed

Mechanical and chemical element structures of sea urchin spines for locomotion and defense

Pathitta Suteecharuwat Corresp., 1, **Mayuka Arakawa** 2, **Yutaka Yoshida** Corresp. 1

[1] Kitami Institute of Technology, Faculty of Engineering, Kitami, Hokkaido, Japan
[2] Kitami Institute of Technology, School of Regional Innovation and Social Design Engineering Intelligent Machines and Biomechanics Course Program, Kitami, Hokkaido, Japan

Corresponding Authors: Pathitta Suteecharuwat, Yutaka Yoshida
Email address: d3227380011@std.kitami-it.ac.jp, yyoshida@mail.kitami-it.ac.jp

Sea urchin spines are of interest for biomaterials and functional materials development due to their mechanical properties, which depend on their elemental composition. However, no previous study has examined the structural distinctions between the spines in the ambulacral and interambulacral areas. This study addresses that gap by investigating the structural and mechanical differences in the spines of *Strongylocentrotus nudus*, with a focus on these two areas. We used cantilever bending tests, Fourier-transform infrared (FT-IR) spectroscopy, X-ray diffraction (XRD), and inductively coupled plasma atomic emission spectroscopy (ICP-AES) to analyze the composition, elasticity, and microstructure of the spines. The bending modulus of elasticity was higher in the ambulacral area (52.067 GPa) compared to the interambulacral area (10.133 GPa), hardness and deformation. ICP-AES analysis revealed that ambulacral shaft had a slightly higher concentration of magnesium (Mg) (0.9844 wt%) compared to the interambulacral shaft (0.9804 wt%), while the calcium (Ca) concentration was lower in the ambulacral shaft (39.6578 wt%) compared to the interambulacral shaft (42.1076 wt%). Furthermore, a variation in Mg concentration was observed between the base and shaft parts of the spine. XRD showed a narrower (104) lattice spacing in the ambulacral spine (3.0264 Å) compared to the interambulacral spine (3.0275 Å), correlating with higher Mg concentration. These compositional and structural differences suggested that *S. nudus* modulates Mg concentration in calcite to achieve functional specialization of spines for locomotion and defense. Our findings may be useful for the development of novel functional materials.

Mechanical and chemical element structures of sea urchin spines for locomotion and defense

Pathitta Suteecharuwat[1], Mayuka Arakawa[2], Yutaka Yoshida[3]

[1] Graduate School of Engineering, Kitami Institute of Technology, Koen-cho, Kitami, Hokkaido 090-8507, Japan
[2] School of Regional Innovation and Social Design Engineering Intelligent Machines and Biomechanics Course Program, Kitami Institute of Technology, Koen-cho, Kitami, Hokkaido 090-8507, Japan
[3] Faculty of Engineering, Kitami Institute of Technology, Koen-cho, Kitami, Hokkaido 090-8507, Japan

Corresponding Author:
Yutaka Yoshida[1]
Koen-cho, Kitami, Hokkaido 090-8507, Japan
Email address: yyoshida@mail.kitami-it.ac.jp

Abstract

Sea urchin spines are of interest for biomaterials and functional materials development due to their mechanical properties, which depend on their elemental composition. However, no previous study has examined the structural distinctions between the spines in the ambulacral and interambulacral areas. This study addresses that gap by investigating the structural and mechanical differences in the spines of *Strongylocentrotus nudus*, with a focus on these two areas. We used cantilever bending tests, Fourier-transform infrared (FT-IR) spectroscopy, X-ray diffraction (XRD), and inductively coupled plasma atomic emission spectroscopy (ICP-AES) to analyze the composition, elasticity, and microstructure of the spines. The bending modulus of elasticity was higher in the ambulacral area (52.067 GPa) compared to the interambulacral area (10.133 GPa), hardness and deformation. ICP-AES analysis revealed that ambulacral shaft had a slightly higher concentration of magnesium (Mg) (0.9844 wt%) compared to the interambulacral shaft (0.9804 wt%), while the calcium (Ca) concentration was lower in the ambulacral shaft (39.6578 wt%) compared to the interambulacral shaft (42.1076 wt%). Furthermore, a variation in Mg concentration was observed between the base and shaft parts of the spine. XRD showed a narrower (104) lattice spacing in the ambulacral spine (3.0264 Å) compared to the interambulacral spine (3.0275 Å), correlating with higher Mg concentration. These compositional and structural differences suggested that *S. nudus* modulates Mg concentration in

calcite to achieve functional specialization of spines for locomotion and defense. Our findings may be useful for the development of novel functional materials.

Introduction

Sea urchins are marine echinoderms with spherical or elliptical shapes and numerous spines on their tests (Johnson et al., 2020). Sea urchin shells and spines are composed of a magnesium (Mg) and calcium (Ca) carbonate structure (Vecchio et al., 2007; Moureaux et al., 2010; Albéric et al., 2019). The spines of *Strongylocentrotus nudus* are composed of stereom structure, a porous, mesh-like microstructure characterized by numerous internal cavities, which make them both lightweight and strong (Moureaux et al., 2010; Gorzelak et al., 2011; Albéric et al., 2019). The mechanical properties of spines depend partly on their constituent elements, such as strength, hardness, and elasticity (Tsafnat et al., 2012; Lauer et al., 2020; Cölfen et al., 2022). These spine structures are expected to be useful in biomaterials and functional materials development because they are optimal for locomotion and defense (Voulgaris et al., 2021; Emerson et al., 2017). Sea urchin tests are ~~distinguished into~~ ambulacral and interambulacral areas (Gao et al., 2015).

The bending behavior of the cantilever is crucial for locomotion as it serves as an indicator of the strength and flexibility of the sea urchin spine. Herein, we examined the relationship between mechanical properties and microstructure using a cantilever bending test and other exact analyses, which indicated that sea urchins control the Mg concentrations to acquire these functions.

In *S. nudus*, spines in the ambulacral area tend to be shorter and thicker. In contrast, those in the interambulacral area are generally longer and thinner, reflecting their distinct roles in locomotion and defense. Tube feet located in the ambulacral area facilitate locomotion across the substrate. During locomotion, the spines support the body by providing mechanical stability and balance. The longer interambulacral spines can radiate outward in response to stimuli, forming a physical barrier that helps deter predators. While the spines respond defensively to touch, locomotion is controlled by the tube feet (Yu et al., 2019; Voulgaris et al., 2021; Thompson et al., 2021; Hebert et al., 2024). Currently, no study has elucidated the structural distinctions between the spines in the ambulacral and interambulacral areas, which are involved in locomotion and defense in sea urchins. Additionally, these spines may have functions other than locomotion and defense. We hypothesized that the two spine types have different functional characteristics. We thus collected the spines of the sea urchin, *S. nudus* and examined them from the ambulacral and interambulacral areas based on their bending properties, crystalline structure, and Mg concentrations. In addition, the structural details were investigated using Fourier-transform infrared (FT-IR) spectroscopy, X-ray diffraction (XRD), and inductively coupled plasma atomic emission spectroscopy (ICP-AES). These structural analyses were performed to determine the relationship between the mechanical properties and constituent elements (Mg and Ca).

Materials & Methods

Sample preparation

Spines of adult sea urchins (*S. nudus*) were procured along with ~~shells~~ from Rishiri Island, Hokkaido Prefecture, Japan. The ~~shells~~ were thoroughly washed, and the organic tissue was removed before being dehydrated at room temperature (25°C). The sea urchin spines were then extracted from the shell by dividing them into ambulacral and interambulacral areas (Figs. 1 and 2) and stored in desiccators at 10^{-2} Pa. Table 1 shows the average spine dimensions, including total length, base length, shaft length, and diameter of the spines.

Cantilever bending test

For the cantilever bending tests, the base of the sea urchin spine was embedded in an aluminum pipe using ultraviolet-hardening acrylate resin. The sea urchin spine ~~in~~ the ambulacral and interambulacral areas was adjusted to an indenter position 1 mm from the spine tip and fixed using a jig for each test (Fig. 3). The loading force and displacement were recorded using an autograph (MX2-500N, ZTA-20N, Imada, Aichi, Japan). In the bending test, 10 spines were used per area. The indenter of a load capability of 20 kN was applied at a 10 mm/min speed. Dimensions such as the total length, base and shaft length, and load point diameter of the sea urchin spines were measured pre- and post-testing. Fractured samples of 10 spines were observed using a digital microscope (VHX-5000; Keyence, Osaka, Japan). The transverse section area of the sea urchin spines, after subtracting the stereom structure, was measured for accurate calculations. The average percentage of the transverse sectional area was 80%. In addition, the bending modulus of elasticity (E), bending strength (σ_B), and maximum bending stress (σ_{max}) were determined using the following equations:

$$E = \frac{\sigma}{\varepsilon} = \frac{F/A}{\Delta L/L} \quad (1)$$

$$\sigma_B = \frac{F(L - x)}{Z} \quad (2)$$

$$\sigma_{max} = \frac{M_{max}}{Z} \quad (3)$$

where, F is the maximum force, A is the transverse section area, ΔL is the displacement, L is the sea urchin spine length, x is the spine position, M_{max} is the maximum bending moment and Z is the section modulus (Moureaux et al., 2010).

Analysis using FT-IR

The spines were split into base and shaft parts and crushed for compound analysis. The size of the powdered spine fragments was between 40 and 100 μm (Fig. 4). For analysis, the powdered samples of each part of the spine were prepared by placing approximately 1 to 5 mg on the plate. Calcite, dolomite, and magnesite in each section were analyzed using an FT-IR spectrometer (FT/IR 500, JASCO, Tokyo, Japan). FT-IR spectra were collected in an infrared reflection area of 30 × 30 μm^2 with a cumulative number of 1,024 times. The wavenumbers ranged from 800 to 1,500 cm^{-1}.

Evaluation of lattice spacing by XRD

To evaluate the lattice spacing by the standard silicon peak at 2θ = 28.4º (Wang et al., 2022), powdered spine samples (0.2 g each) were prepared with 10% silicon powder for each part of the spine. The exact 2θ of the calcite (104) and (006) planes in the spine was measured using an X-ray diffractometer (Rigaku Ultima IV, Tokyo, Japan). The diffractometer was operated at 40 kV and 40 mA at a 2θ range of 27–33° with a step size of 0.01° (Cu-Kα radiation: λ = 1.5418 Å). Then, the peaks (104) and (006) planes were determined by Lorentzian fitting software (OriginPro, Northampton, Massachusetts). The lattice spacing (*d*) of the spine was calculated using Bragg's law, as follows:

$$d = \frac{\lambda}{2 sin\,\theta} \quad (4)$$

where λ is the wavelength of X-ray radiation, and θ is the diffraction angle.

Trace element analysis by ICP-AES

First, each powdered spine sample (0.1 g) was placed in an airtight container with 2 mL of Nitric acid (HNO_3), and dissolved by heating at 100℃ for 40 min. Second, the dissolved samples were cooled to room temperature (20–25°C), and pure water was added to make up a volume of 50 mL. The mixed samples were diluted 2,000-fold with pure water to the weight of Ca and 100-fold to the weight of Mg. For calibration, the standard solutions of Ca and Mg were diluted from 1,000 ppm to 5, 2.5, 1, 0.5, 0.25, 0.1, 0.05, 0.025, and 0.01 ppm. Finally, the trace elements were analyzed using ICP-AES (SPS3100HV UV, SII, Japan). The samples of each part were measured using ICP-AES under conditions of high-frequency power (1.2 kW), and a cumulative number of 5 times. The concentrations of Ca and Mg in each part were measured, and the corresponding quantity (wt%) was calculated as follows:

$$wt\% = \left(\frac{M_C \times V \times D \times S_C}{M}\right) \times 100 \quad (5)$$

Where, M_C is the mass of the concentration, V is the volume to be increased, D is the dilution ratio, S_C is the standard solution concentration, and M is the mass of the sample.

Results

Cantilever bending test

Fig. 5 shows the force-displacement diagram of one representative spine per area for the cantilever bending test. The mechanical behavior of the fracture was linear, and the average maximum force and displacement were determined from this relationship. Fractures occurred in the middle of three spines, in the tip of seven spines for the ambulacral area, and in the tip of 10 spines for the interambulacral areas. The average maximum force in the ambulacral spine was 1.2350 N, while in the interambulacral spine it was 0.9180 N. The average displacement in the ambulacral spine was 1.3265 mm, and in the interambulacral spine, it was 4.7523 mm. Table 2 lists the mechanical properties of spines in the ambulacral and interambulacral areas. The average bending modulus of spine elasticity in the ambulacral and interambulacral areas was 52.067 GPa and 10.133 GPa, respectively. The average bending strength of the spine in the ambulacral area was 631.75 MPa and 300.71 MPa in the interambulacral area. The average maximum stress of the spine in the ambulacral area was 1,822.77 MPa and 1,554.89 MPa in the interambulacral area.

FT-IR analysis

Fig. 6 shows the FT-IR spectra of the (a) base and (b) shaft of sea urchin spines. Fig. 6(a) shows that in the base of the spine in the ambulacral and interambulacral areas, calcite peaks appeared at 1,419 and 1,410 cm^{-1}, while magnesite peaks appeared at 855 and 861 cm^{-1}. Fig. 6(b) shows the magnesite peak in the shaft part appeared at 860 and 855 cm^{-1}, while the calcite peak appeared at 1,418 and 1,420 cm^{-1} (Vecchio et al., 2007; Tanaka et al., 2019). The dolomite peak occurred at 888 cm-1 for both base and shaft part in both areas (Bruckman and Wriessnig, 2013).

Evaluation of lattice space using XRD

Fig. 7 shows the XRD patterns of powdered sea urchin spine samples from each part of both areas. The peaks of the (104) plane appeared as follows (Borzęcka-Prokop et al., 2007): the base parts in the ambulacral and interambulacral areas were at 29.512° and 28.498°, respectively. The shaft angles in the ambulacral and interambulacral areas were 29.479 °and 29.475°, respectively. The (006) peaks appeared as follows: the bases in the ambulacral and interambulacral areas were 31.581° and 31.563°, respectively. The shaft angles in the ambulacral and interambulacral areas were 31.529° and 31.544°, respectively. Fig. 8 shows the lattice spacing of the sea urchin spines from each part in both areas. The lattice spacing increased from the base to the shaft in both areas. In the base part of the (104) plane, the lattice spacing in the ambulacral area was narrower than that in the interambulacral area. The average lattice spacing of the (104) plane of the base part in the ambulacral and interambulacral areas were 3.0231 and 3.0238 Å, respectively. The average lattice spacing of the shaft part in the ambulacral and interambulacral areas were 3.0264 and 3.0275 Å, respectively.

Trace element analysis

Fig. 9 show the average concentrations (wt%) of Ca and Mg contained in each part of the spine from the ambulacral and interambulacral areas. In both areas, the Ca concentration in the base was lower than that of the shaft, while the Mg concentration was higher in the base compared to the shaft. In the base part of the spine, Ca concentration in the ambulacral area (35.4173%) was higher compared to the interambulacral area (31.6537%). The Mg concentration in the ambulacral area (1.1532%) was lower compared to that in the interambulacral area (1.2091%). In the shaft part of the spine, Ca concentration in the ambulacral area (39.6578%) was lower compared to that in the interambulacral area (42.1076%) while the Mg concentration was slightly higher in the ambulacral area (0.9866%) compared to that in the interambulacral area (0.9804%).

Discussion

In this study, we investigated the relationship between the mechanical properties and constituent elements in the ambulacral and interambulacral areas of *S. nudus* spines, focusing on their roles in locomotion and defense. Our analyses revealed differences in both the structural and compositional characteristics of the spines in the ambulacral and interambulacral areas. The spines in the ambulacral area demonstrated increased hardness and decreased elasticity, contributing to increased locomotory support by the tube feet. In contrast, the spines in the interambulacral area showed higher bending capacity and elasticity, a structure more suitable for defense through rapid outward extension in response to external stimuli (Moureaux et al., 2010; Tsafnat et al., 2012).

ICP and XRD analyses showed that the base of the spine generally contained more Mg than the shaft, suggesting that base strengthening is related to modifications in the crystalline lattice spacing in the (104) cleavage plane (Deng et al., 2022). The lattice spacing in the ambulacral area was narrower than that in the interambulacral area, and the Mg concentration in the base of ambulacral spines was lower than in the interambulacral spines. However, the Mg concentration was higher in the shaft of the ambulacral area. The Mg distribution suggests functional specialization in the ambulacral area. The mechanical strength of the base, attributed to increased hardness from its crystalline structure, is crucial for protecting the organism (Magdans and Gies, 2004).

Damage to the base of the spine is often fatal, highlighting the importance of vital protection in this region (Moureaux et al., 2010; Gorzelak et al., 2011; Albéric et al., 2019). The increasing Mg concentration in the shaft is identified with narrower lattice spacing, referring to solid-solution strengthening where Mg displaces Ca, transforming calcium carbonate into magnesium carbonate and dolomite (Lauer et al., 2020; Deng et al., 2022). This results in increased maximum bending stress, which may enhance performance during locomotion.

Our results support the hypothesis that echinoid spines are structurally and functionally specialized based on the ambulacral and interambulacral areas, and in the base and shaft parts. Previous studies have detailed stereom structure and mineral composition (Moureaux et al., 2010; Cölfen et al., 2022), but our study is among the first to correlate microstructural differences with mechanical function between spine types. The observed variation in Mg concentration is consistent with previous findings, which links higher Mg levels to increased hardness in calcite (Albéric et al., 2019).

Controlling Mg concentration may function as a biological method to optimize mechanical properties by optimizing the hardness and elasticity. The orientation of crystalline domains in interambulacral spines may also contribute to their controlled elasticity under mechanical stress.

Understanding how Mg concentration and microstructure affect mechanical properties in sea urchin spines provides valuable insight into the design of bioinspired materials that combine transformability with strength (Magdans and Gies, 2004; Moureaux et al., 2010).
While our study is limited by analysis and may not fully capture living behavior, it nonetheless provides a foundational understanding of how microstructural and compositional factors, such as Mg concentration, affect echinoderm biomechanics. These findings offer a strong basis for future investigations. Future research should investigate environmental factors, such as seawater chemistry, control of Mg concentration, and examine the genetic regulation of the biomineralization mechanism. Moreover, investigating whether sea urchin spines are transformed in response to fracture or biological stress could reveal important transformative mechanisms. Comparative studies across different echinoid species may also provide valuable evolutionary insights into the functional specialization and morphological diversity of spines.

Conclusions

This study provides an extensive analysis of the mechanical properties and constituent elements of sea urchin (*S. nudus*) spines, exhibiting substantial Mg concentration in the different functional areas between ambulacral and interambulacral areas. The higher Mg concentration in ambulacral spines results in increased hardness and narrow lattice spacing to improve support during locomotion. In contrast, the lower Mg concentration in interambulacral spines confers elasticity to resist cleavage fractures, optimizing them for defensive functions. These observations reveal how solid-solution strengthening and microstructural variations contribute to the functionality of a single biological structure (Seto et al., 2012; Deng et al., 2022).
The specialized mechanical properties observed in sea urchin spines reveal important evolutionary adaptations and offer a compelling model for developing advanced biomaterials. Future research into atomic-level structure, compressive strength, and environmental influences on Mg concentration in sea urchin spine could further inform the design of bioinspired materials with tunable mechanical properties. These results have the potential to contribute to innovations in biomaterials and functional materials.

Acknowledgements

We would like to thank N. Takeda, Instrumental Analysis Division, Global Facility Center, Creative Research Institution, Hokkaido University, for advice. We also thank Hashimoto, Kitami Institute of Technology, open facility center for analyzing sea urchin spines using inductively coupled plasma atomic emission spectroscopy, Fourier-transform infrared spectroscopy, and X-ray diffraction, to provide insights and expertise that greatly assisted this research.

References

Albéric M, Stifler CA, Zou Z, Sun YC, Killian CE, Valencia S, Mawass MA, Bertinetti L, Gilbert P, Politi Y. 2019. Growth and regrowth of adult sea urchin spines involve hydrated and anhydrous amorphous calcium carbonate precursors. Journal of Structural Biology: X 1: 100004 https://doi.org/10.1016/j.yjsbx.2019.100004

Borzęcka-Prokop B, Wesełucha-Birczyńska A, Koszowska E. 2007. MicroRaman, PXRD, EDS, and microscopic investigation of magnesium calcite biomineral phases: The case of sea urchin biominerals. Journal of Molecular Structure 828(1–3): 80–90 https://doi.org/10.1016/j.molstruc.2006.05.040

Bruckman VJ, Wriessnig K. 2013. Improved soil carbonate determination by FT-IR and X-ray analysis. Environmental Science and Pollution Research 11: 65–70 https://doi.org/10.1007/s10311-012-0380-4

Cölfen H, Bürgi HB, Chernyshov D, Stekiel M, Chumakova A, Bosak A, Wehinger B, Winkler B. 2022. Mesocrystalline structure and mechanical properties of biogenic calcite from sea urchin spine. Physics of the Solid State 57(3): 1094–1104 https://doi.org/10.1007/s11041-021-00490-7

Deng Z, Jia Z, Li L. 2022. Biomineralized materials as model systems for structural composites: Intracrystalline structural features and their strengthening and toughening mechanisms. Advanced Science 9(14): 2103524 https://doi.org/10.1002/advs.202103524

Emerson CE, Reinardy HC, Bates NR, Bodnar AG. 2017. Ocean acidification impacts spine integrity but not regenerative capacity of spines and tube feet in adult sea urchins. Royal Society Open Science 4: 170140 https://doi.org/10.1098/rsos.170140

Gao F, Thompson JR, Petsios E, Erkenbrack E, Moats RA, Bottjer DJ, Davidson EH. 2015. Juvenile skeletogenesis in anciently diverged sea urchin clades. Developmental Biology 400(1): 148–158 https://doi.org/10.1016/j.ydbio.2015.01.017

Gorzelak P, Stolarski J, Dubois P, Kopp C, Meibom A. 2011. 26Mg labeling of the sea urchin regenerating spine: Insights into echinoderm biomineralization process. Journal of Structural Biology 176(1): 119–126 https://doi.org/10.1016/j.jsb.2011.07.008

Hebert E, Silvia M, Wessel GM. 2024. Structural and molecular distinctions of primary and secondary spines in the sea urchin Lytechinus variegatus. Scientific Reports 14: 28525 https://doi.org/10.1038/s41598-024-76239-7

Lauer C, Haußmann S, Schmidt P, Fischer C, Rapp D, Berthold C, Nickel KG. 2020. On the relation of amorphous calcium carbonate and the macromechanical properties of sea urchin spines. Advanced Engineering Materials 22(4): 1900922 https://doi.org/10.1002/adem.201900922

Magdans U, Gies H. 2004. Single crystal structure analysis of sea urchin spine calcites: Systematic investigations of the Ca/Mg distribution as a function of habitat of the sea urchin and the sample location in the spine. European Journal of Mineralogy 16: 261–268 https://doi.org/10.1127/0935-1221/2004/0016-0261

Moureaux C, Pérez-Huerta A, Compère P, Zhu W, Leloup T, Cusack M, Dubois P. 2010. Structure, composition and mechanical relations to function in sea urchin spine. Journal of Structural Biology 170(1): 41–49 https://doi.org/10.1016/j.jsb.2010.01.003

Roberta J, Harianto J, Thomson J, Byrne M. 2020. The effects of long-term exposure to low pH on the skeletal microstructure of the sea urchin Heliocidaris erythrogramma. Journal of

Experimental Marine Biology and Ecology 523: 151250 https://doi.org/10.1016/j.jembe.2019.151250

Seto J, Ma Y, Davis SA, Meldrum F, Gourrier A, Kim Y-Y, Schilde U, Sztucki M, Burghammer M, Maltsev S, Jäger C, Cölfen H. 2012. Structure–property relationships of a biological mesocrystal in the adult sea urchin spine. Proceedings of the National Academy of Sciences 109: 3699–3704 https://doi.org/10.1073/pnas.1109243109

Tanaka J, Kawano J, Nagai T, Teng H. 2019. Transformation process of amorphous magnesium carbonate in aqueous solution. Journal of Mineralogical and Petrological Sciences 114(2): 105–109 https://doi.org/10.2465/jmps.181119b

Thompson JR, Paganos P, Benvenuto G, Arnone MI, Oliveri P. 2021. Post-metamorphic skeletal growth in the sea urchin Paracentrotus lividus and implications for body plan evolution. EvoDevo 12: 3 https://doi.org/10.1186/s13227-021-00174-1

Tsafnat N, Fitz Gerald JD, Le HN, Stachurski ZH. 2012. Micromechanics of sea urchin spines. PLoS ONE 7(9): e44140 https://doi.org/10.1371/journal.pone.0044140

Vecchio KS, Zhang X, Massie JB, Wang M, Kim CW. 2007. Conversion of sea urchin spines to Mg-substituted tricalcium phosphate for bone implants. Acta Biomaterialia 3(5): 785–793 https://doi.org/10.1016/j.actbio.2007.03.009

Voulgaris K, Varkoulis A, Zaoutsos S, Stratakis A, Vafidis D. 2021. Mechanical defensive adaptations of three Mediterranean sea urchin species. Ecology and Evolution 11: 17734–17743 https://doi.org/10.1002/ece3.8247

Wang C, Niu X, Wang D, Zhang W, Shi H, Lu Y, Wang C, Xiong Z, Ji Z, Yan X, Gu Y. 2022. Simple preparation of Si/CNTs/C composite derived from photovoltaic waste silicon powder as high-performance anode material for Li-ion batteries. Powder Technology 408: 117744 https://doi.org/10.1016/j.powtec.2022.117744

Yu H, Lin T, Xin Y, Li J, Li J, Chen Y, Chen X, Liu L. 2019. Strengthening the mechanical performance of sea urchin skeleton by tube feet pore. Journal of Ocean University of China 16: 66–75 https://doi.org/10.1007/s42235-019-0007-6

Figure 1

Fig. 1. Sea urchin *Strongylocentrotus nudus*

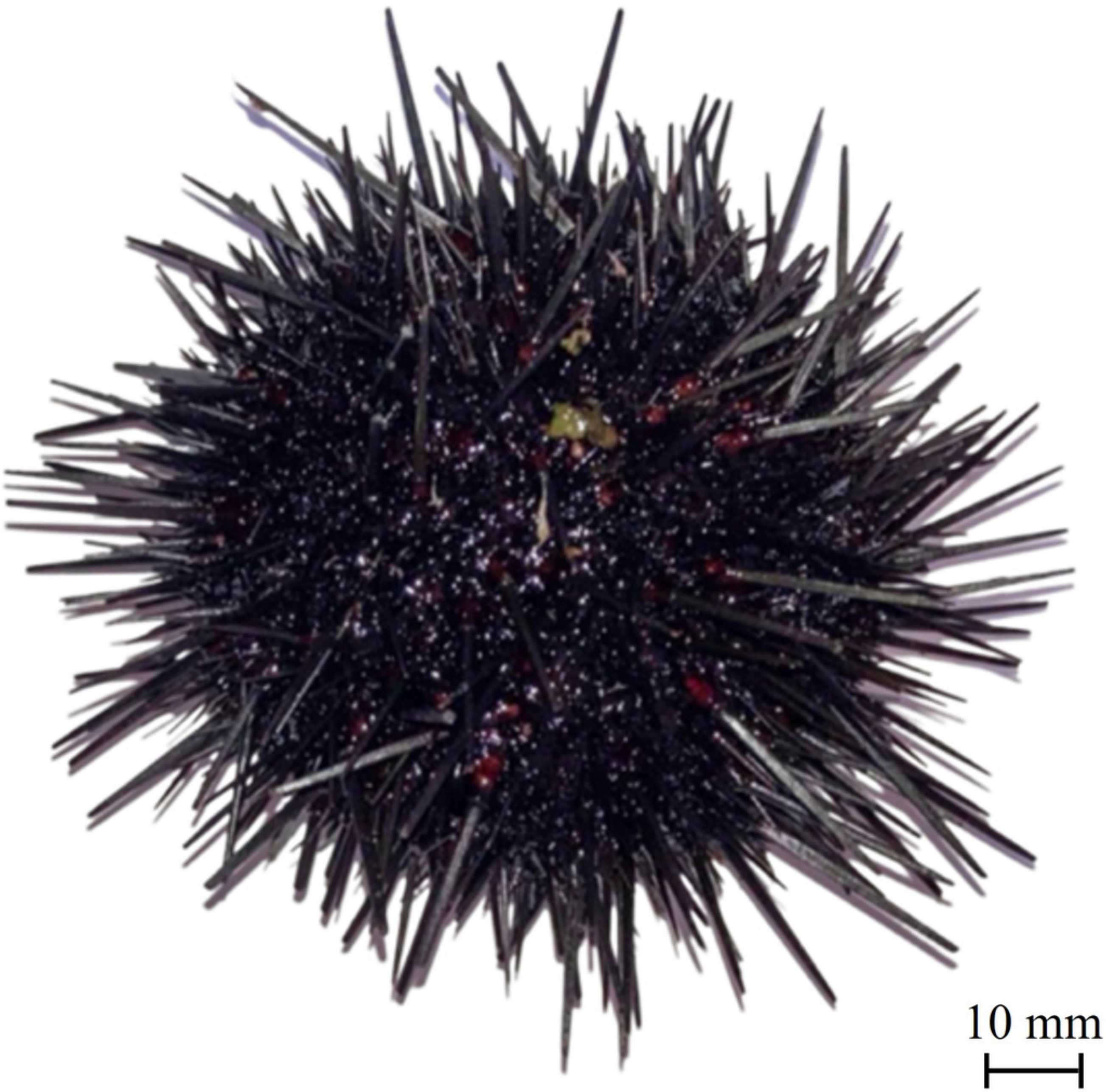

Figure 2

Fig. 2. Sea urchin spines in the a) *ambulacral* and b) *interambulacral* areas

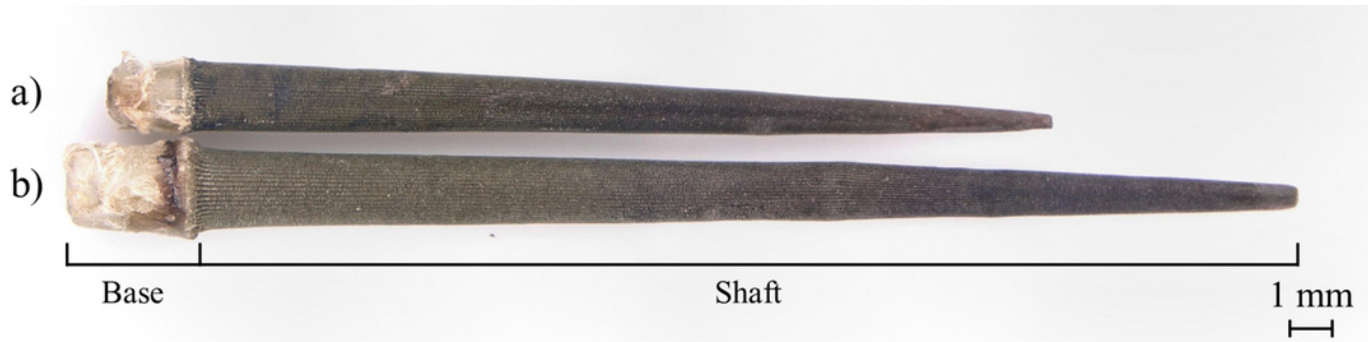

Figure 3

Fig. 3. Sea urchin spines fixed using a jig for the bending test

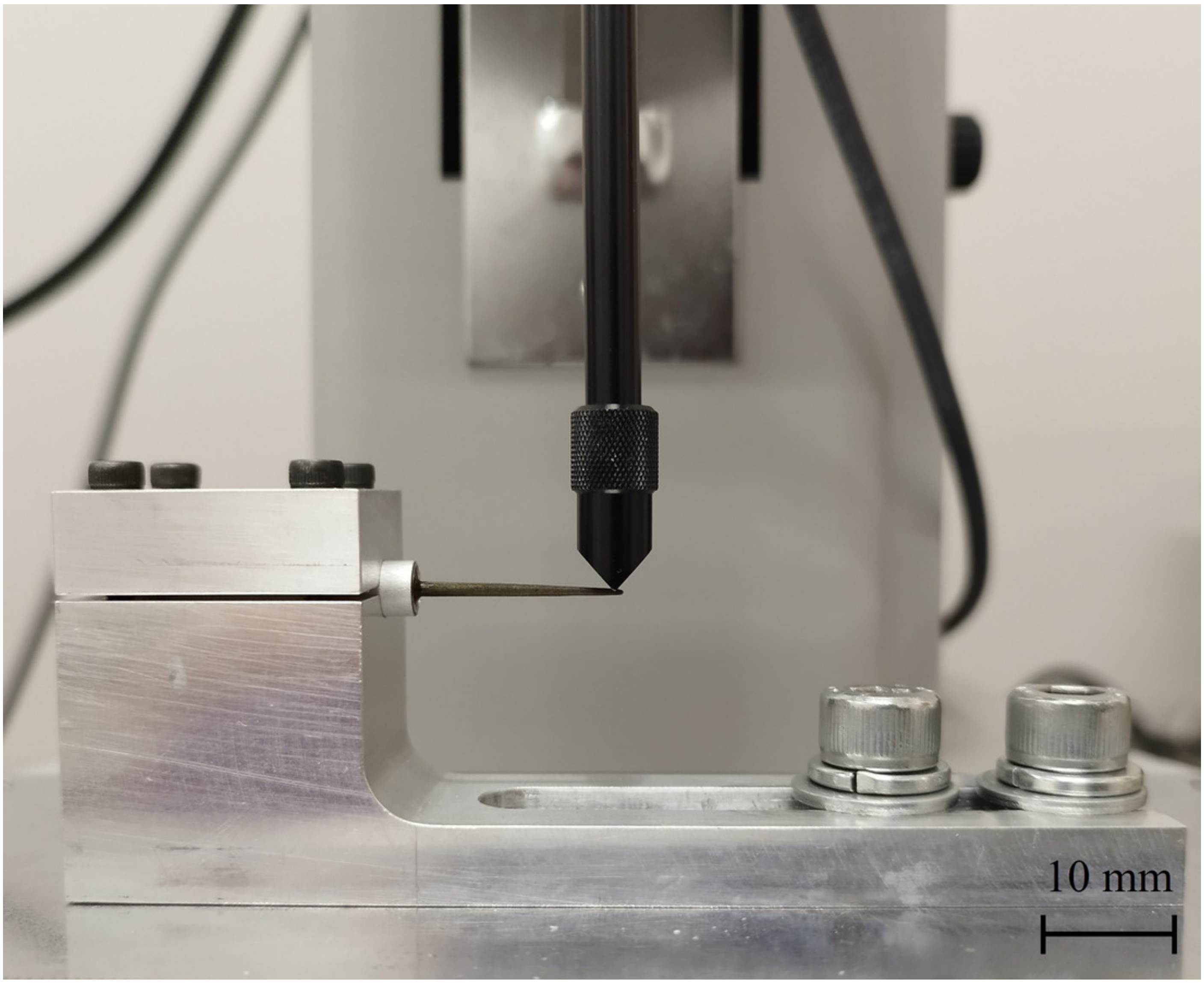

Figure 4

Fig. 4. Powder sample of sea urchin spine

Figure 5

Fig. 5. Force-Displacement diagram of one representative spine from each area

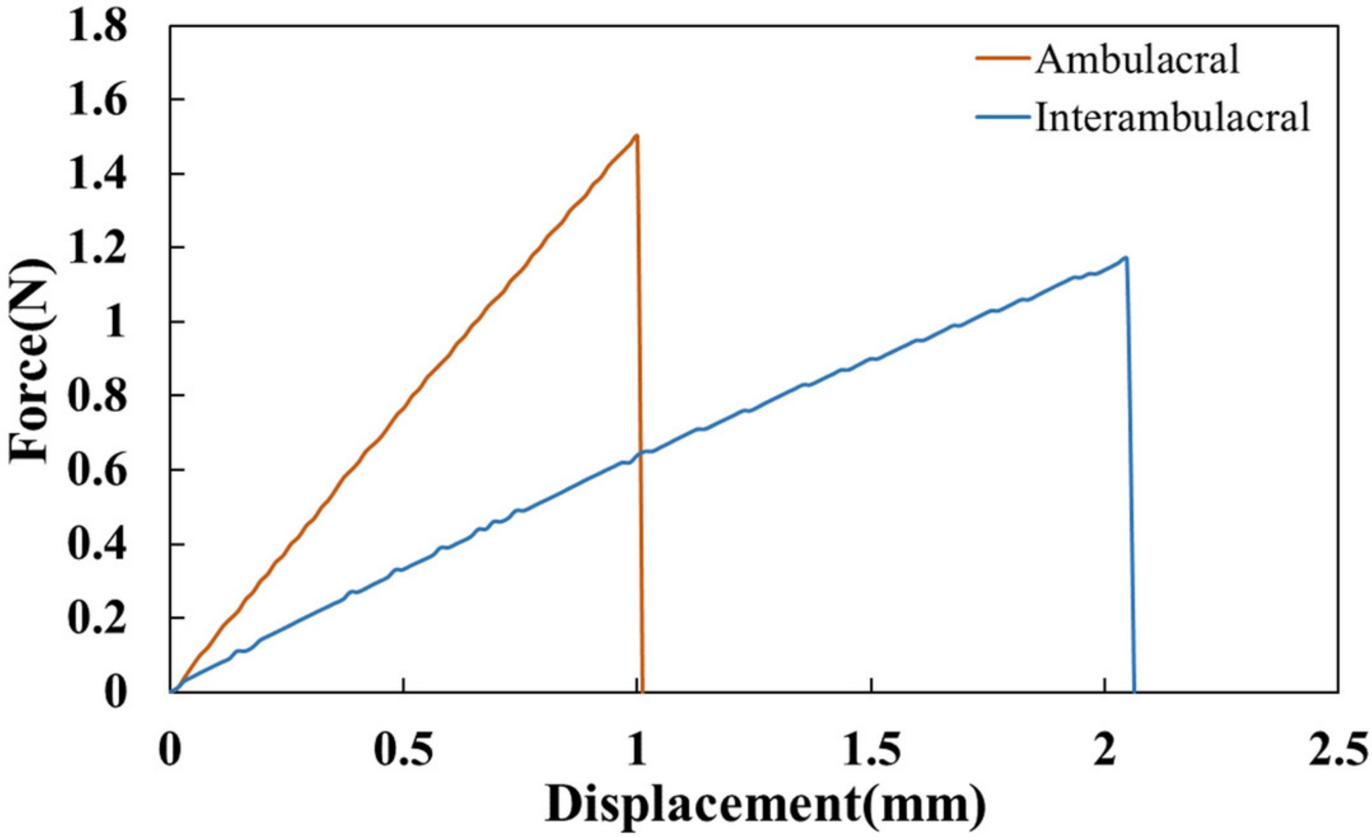

Figure 6

Fig. 6. Fourier-transform infrared (FT-IR) spectra of the (a) base and (b) shaft of sea urchin spines in a wavenumber range of 800–1500 cm^{-1}

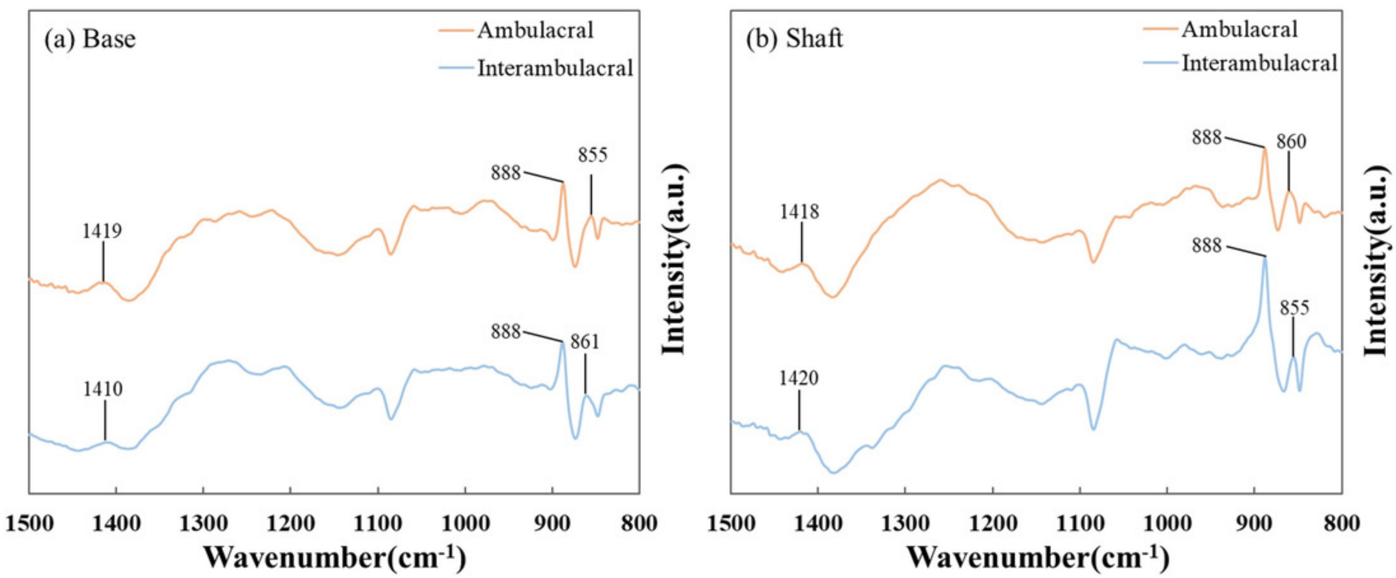

Figure 7

Fig. 7. X-ray diffraction (XRD) patterns of the sea urchin spine from (a) base and (b) shaft in the ambulacral and interambulacral areas

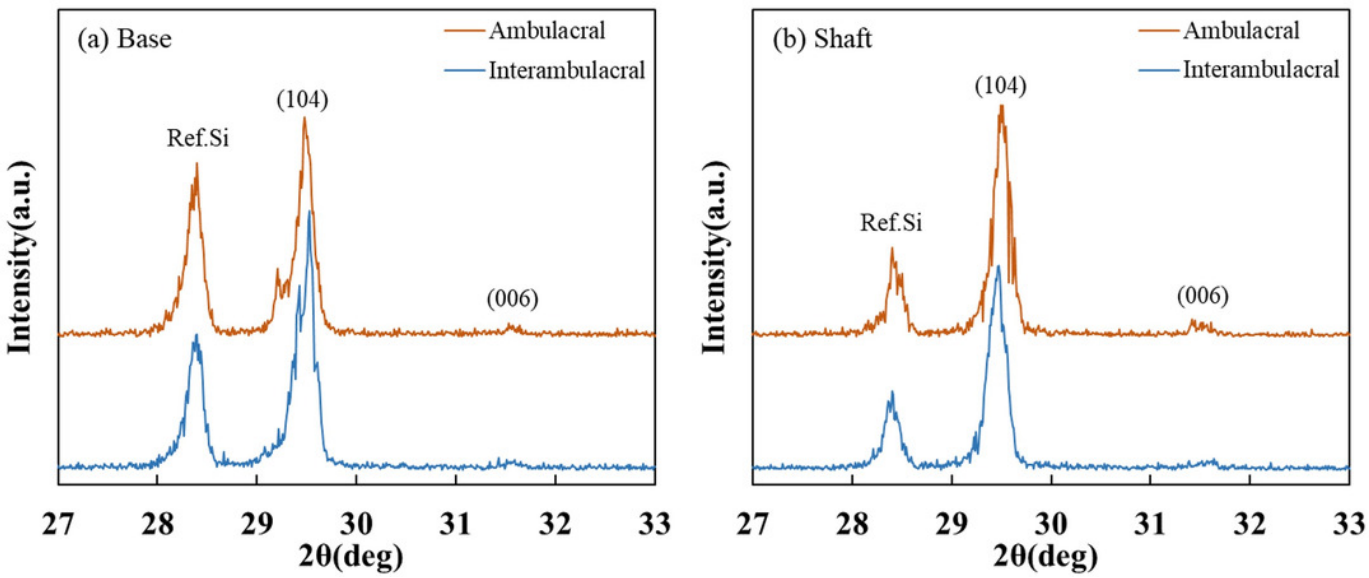

Figure 8

Fig. 8. Lattice space of (104) plane from the base and shaft in the ambulacral and interambulacral areas

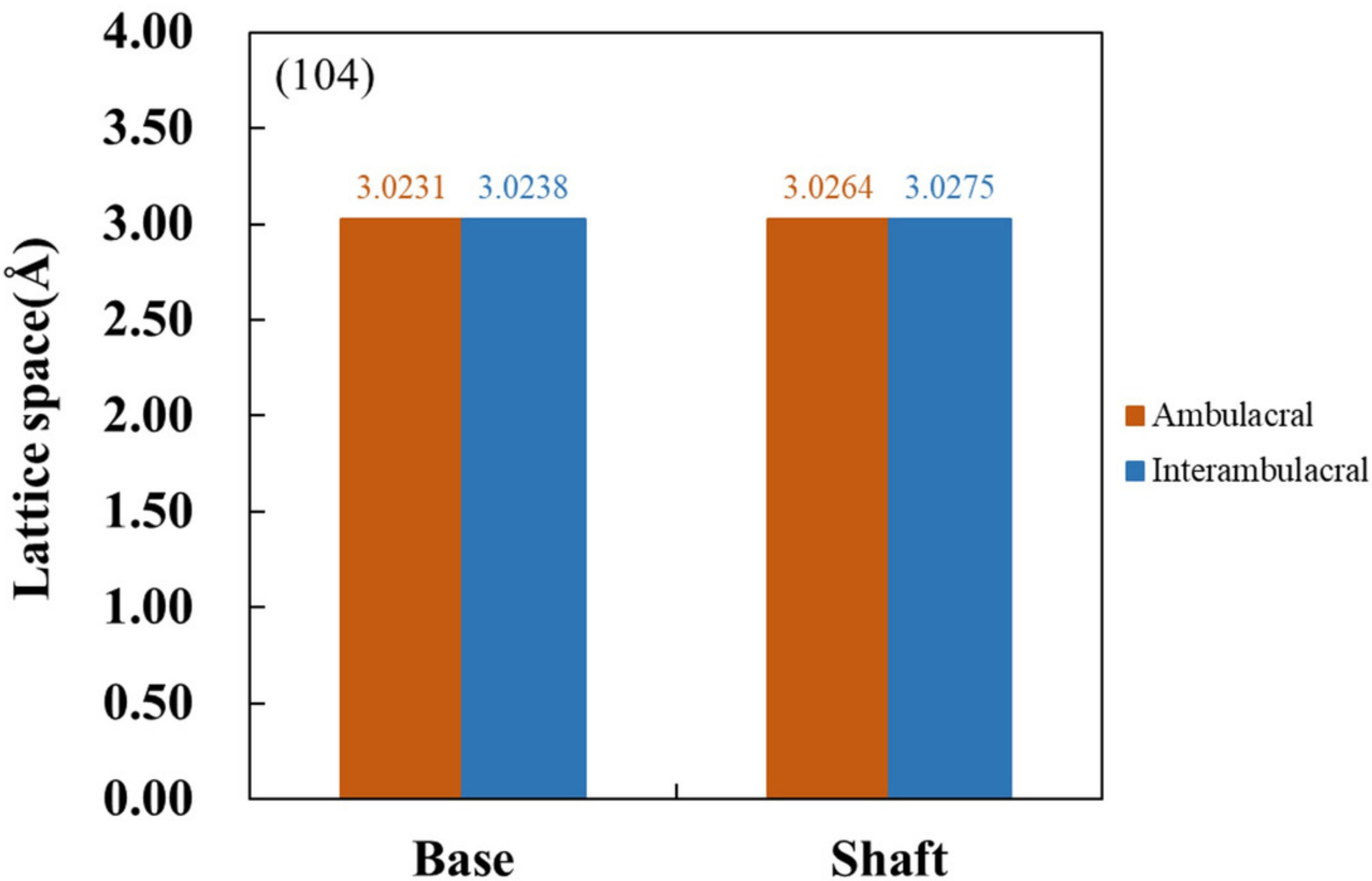

Figure 9

Fig. 9. Inductively coupled plasma atomic emission spectroscopy (ICP-AES) wt% of (a) calcium and (b) magnesium in the base and shaft in the ambulacral and interambulacral areas

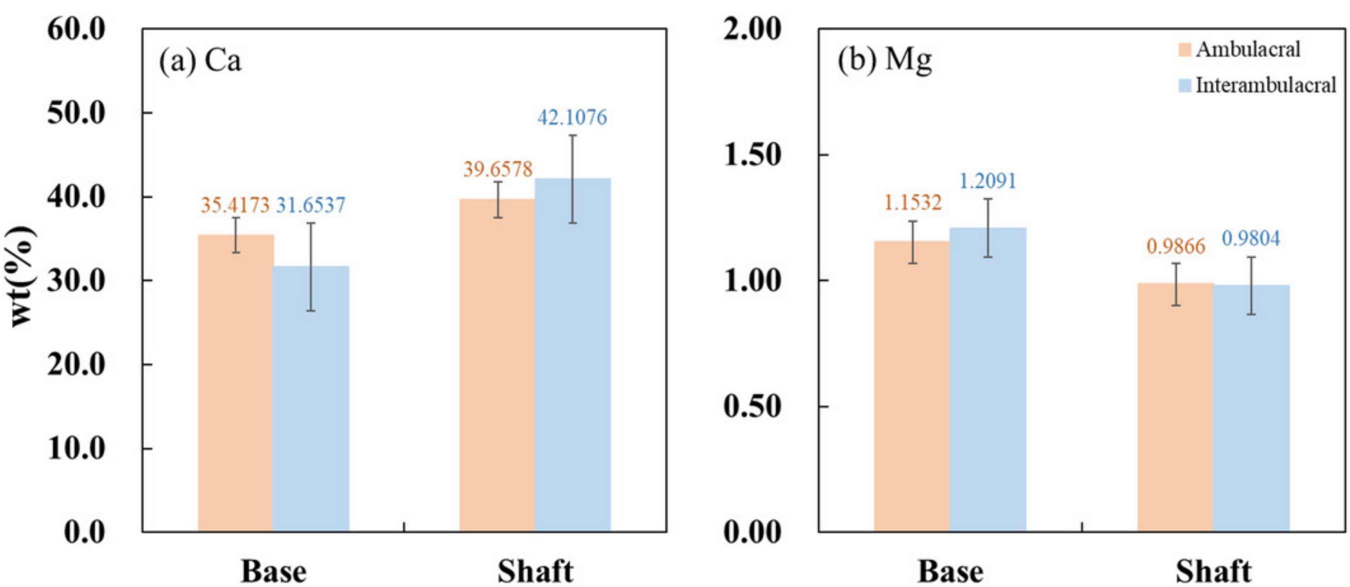

Table 1(on next page)

Table 1: Dimensions of sea urchin spines on *Strongylocentrotus nudus* (n=10 per area)

Table 1: Dimensions of sea urchin spines on *Strongylocentrotus nudus* (n=10 per area)

	Total length (mm)	Base length (mm)	Shaft length (mm)	Diameter (mm)
Ambulacral area	23.73 ± 2.45	2.08 ± 0.37	21.71 ± 2.15	0.52 ± 0.07
Interambulacral area	33.61 ± 3.97	2.88 ± 0.58	30.71 ± 3.40	0.59 ± 0.11

Table 2 (on next page)

Table 2: Mechanical properties of sea urchin spines

Table 2: Mechanical properties of sea urchin spines

	Ambulacral	Interambulacral
Bending modulus (GPa), E	52.067	10.133
Bending strength (MPa), σ_B	631.75	300.71
Maximum stress (MPa), σ_{max}	1822.77	1554.89